Ground and Electronically Excited Singlet-State Structures of 5-Fluoroindole Deduced from Rotationally Resolved Electronic Spectroscopy and ab Initio Theory

Christian Brand,[a] Olivia Oeltermann,[a] Martin Wilke,[a] Jörg Tatchen,[b] and Michael Schmitt*[a]

The structure and electronic properties of the electronic ground state and the lowest excited singlet state (S_1) of 5-fluoroindole (5FI) were determined by using rotationally resolved spectroscopy of the vibration-less electronic origin of 5FI. From the parameters of the axis reorientation Hamiltonian, the absolute orientation of the transition dipole moment in the molecular frame was determined and the character of the excited state was identified as L_b.

1. Introduction

The electronic properties of the aromatic chromophore indole strongly depend on the nature of the substituents and the local surroundings. The two lowest excited singlet states (called L_a and L_b in the nomenclature of Platt)[1] might even change their energetic order, depending on the polarity of the local surroundings. These surroundings can be made up from a matrix; solvent molecules, which form complexes with the chromophore; or flexible substituents, which can interact with the chromophore by through-bond or -space interactions.[2–4] Recently, we have shown that the introduction of a cyano group, which exerts a strong negative mesomeric (−M) effect in the 5-position of the indole ring [(5-cyanoindole (5CI)], shifts the L_a state below the L_b.[5] In the present work, we investigate the effect of a purely negative inductive (−I) effect in the 5-position, as exerted by a fluorine substituent.

A thorough vibrational and vibronic analysis of the three 4-, 5-, and 6-fluoroindoles has been given by Barstis et al.[6] based on jet-cooled, one-color resonant, two-photon ionization, time-of-flight mass spectrometry (R2PI TOF-MS). Huang and Sulkes[7] reported the origin frequency using R2PI TOF-MS and the fluorescence lifetime of 5-fluoroindole (5FI) from time-correlated single-photon counting for S_1 state levels. Their value of 33 911 cm^{-1}[7] for ν_0 deviates by 431 cm^{-1} from the value reported by Barstis et al.[6] Herein, we record a value of 425 cm^{-1}, which supports that reported by Barstis et al.[6]

Experimental Section

5FI ($\geq$ 98 %) was purchased from Activate Scientific and used without further purification. The experimental setup for the rotationally resolved laser-induced fluorescence is described in detail elsewhere.[8] In brief, the laser system consisted of a single-frequency ring dye laser (Sirah Matisse DS) operated with rhodamine 6G, pumped with 7 W of the 514 nm line of an Ar$^+$ ion laser (Coherent, Sabre 15 DBW). The dye laser output was coupled into an external folded ring cavity (Spectra Physics Wavetrain) for second-harmonic generation. The resulting output power was constant at about 15 mW during the experiment. The molecular beam was formed by co-expanding 5FI, heated to 45 °C, and 500 mbar of argon through a 200 µm nozzle into the vacuum chamber. The molecular beam machine consisted of three differentially pumped vacuum chambers that were linearly connected by skimmers (1 mm and 3 mm, respectively) to reduce the Doppler width. The resulting resolution was 18 MHz (FWHM) in this setup. In the third chamber, 360 mm downstream of the nozzle, the molecular beam crossed the laser beam at a right angle. The imaging optics setup consisted of a concave mirror and two planoconvex lenses to focus the resulting fluorescence onto a photomultiplier tube, which was mounted perpendicularly to the plane defined by the laser and molecular beam. The signal output was then discriminated and digitized by a photon counter and transmitted to a PC for data recording and processing. The relative frequency was determined with a quasi confocal Fabry–Perot interferometer. The absolute frequency was obtained by comparing the recorded spectrum to the tabulated lines in the iodine absorption spectrum.[9]

Computational Methods

Quantum Chemical Calculations

All calculations were performed with the Turbomole program package.[10, 11] Dunning's correlation consistent polarized valence triple zeta (cc-pVTZ) basis sets from the Turbomole library were used.[12] The equilibrium geometries of the electronic ground and the lowest excited singlet states were optimized by using the approximate coupled cluster singles and doubles model (CC2), employing the resolution-of-the-identity approximation (RI).[13–15] Spin-component scaling (SCS) modifications to CC2 were also taken into ac-

[a] C. Brand, O. Oeltermann, M. Wilke, Prof. Dr. M. Schmitt
Heinrich-Heine-Universität
Institut für Physikalische Chemie I
40225 Düsseldorf (Germany)
E-mail: mschmitt@uni-duesseldorf.de

[b] Prof. Dr. J. Tatchen
Heinrich-Heine-Universität
Institut für Theoretische Chemie
40225 Düsseldorf (Germany)

count.[16] Vibrational frequencies and zero-point corrections to the adiabatic excitation energies have been obtained from numerical second derivatives by using the NumForce script.[11] Natural population analyses (NPA)[17] were performed at the CC2-optimized geometries by using the wave functions from the CC2 calculations implemented in the Turbomole package.[11]

Fits of the Rovibronic Spectra Using Evolutionary Algorithms

We make use of an evolutionary strategy (ES), namely, the covariance matrix adaptation ES (CMA-ES) for the fit of the rovibronic spectrum. This algorithm was developed by Ostenmeier and Hansen.[18,19] It belongs, like the other search algorithms employed in our group, to the class of global optimizers inspired by evolutionary processes. For a detailed description of these evolutionary and genetic strategies for fitting of molecular spectra, see refs. [20] and [21].

2. Results and Discussion

2.1. High-Resolution Spectrum of the Origin Band of 5FI

Figure 1 shows the rotationally resolved spectrum of the electronic origin of 5FI at 34 342 cm^{-1}. The experimental spectrum
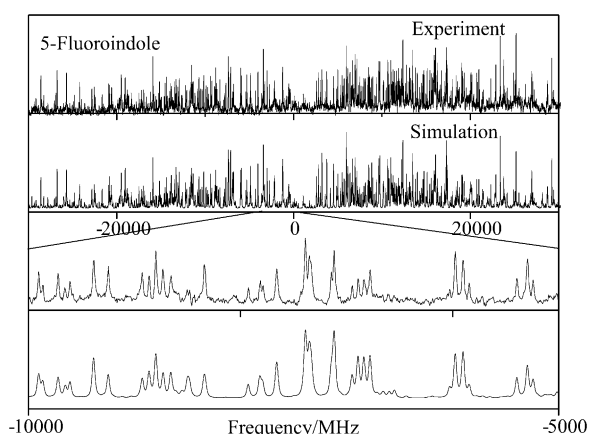
Figure 1. Rotationally resolved electronic spectrum of the electronic origin of 5FI.

could be simulated with a rigid rotor Hamiltonian, containing axis reorientation[22,23] and *ab*-hybrid-type selection rules with 27% *a*-type and 73% *b*-type. For molecules with less than C_{2v} symmetry, the geometry changes upon electronic excitation rotate the inertial axis system. For a planar molecule, this rotation can be described by using a single rotational angle θ_T. In 5FI, the *c*-axis is perpendicular to the aromatic plane, and θ_T describes the rotation of the *a''* axis of the ground state onto the *a'* axis of the excited state about the *c* axis. This axis reorientation angle is defined in Figure 2. A magnified portion of the spectrum shows the excellent agreement between experiment and simulation when using the parameters from the best fit from the CMA-ES strategy. The fit of the line shapes to Voigt profiles using a Gaussian (Doppler) contribution of 18 MHz
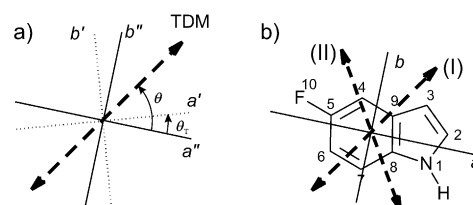
Figure 2. a) Definition of the positive direction of the transition dipole moment (TDM) angle, θ, and of the axis reorientation angle, θ_T. b) Atomic numbering of 5FI and orientation of the inertial axes and the two possible TDM orientations.

yielded a Lorentzian contribution of (13 ± 2) MHz to the total line width, equivalent to an excited-state lifetime of (12 ± 4) ns.

Different thermalization of the JK_AK_c states in a molecular beam requires a description of populations at several temperatures, which take into account the dependence of rotational cooling on angular momentum. We used the two-temperature model, proposed by Wu and Levy[24] with $n_i = e^{-E_i/kT_1} + we^{-E_i/kT_2}$, in which n_i is the population of the *i*th rovibronic level at energy E_1, k is the Boltzmann constant, T_1 and T_2 are the two temperatures, and w is a weighting factor that models the contribution from T_2. The best agreement between experimental and simulated spectra could be obtained with $T_1 = 2.5$ K, $T_2 = 4.8$ K, and $w = 0.2$.

The results of the fit are compiled in Table 1. Apart from the rotational constants, which contain information about the

Table 1. CC2/cc-pVTZ-calculated molecular parameters of 5FI versus experimental values. Changes of the rotational constants are defined as $\Delta B_g = B_g^{\&} - B_g^{'\&}$, with B_g as rotational constants with respect to the inertial axes $g = a$, b, and c. The ab initio calculated constants represent equilibrium values, whereas the experimental constants are zero-point vibrationally averaged. More details are given in the text.

	CC2/cc-pVTZ	exp.
A'' [MHz]	3520	3519.57(4)
B'' [MHz]	1019	1019.79(1)
C'' [MHz]	790	790.87(1)
$\Delta I''$ [amu Å^2]	0.0	−0.1487
A' [MHz]	3395	3386.34(3)
B' [MHz]	1018	1019.83(1)
C' [MHz]	783	784.09(1)
$\Delta I'$ [amu Å^2]	0.0	−0.2468
ΔA [MHz]	−125	−133.23(2)
ΔB [MHz]	−1	+0.043(1)
ΔC [MHz]	−7	−6.78(1)
θ [°]	±40	±59(1)
θ_T [°]	±0.65	±0.8(1)
ν_0 [cm^{-1}]	35 144	34 335.89(1)

structure of the molecule in both electronic states, the TDM orientation, measured by the angle θ is also obtained. Although its sign is undetermined (see Section 2.2 below), the axis reorientation Hamiltonian yields the relative signs of θ and θ_T as ±. This means that if θ is positive θ_T will also be positive and vice versa. By using information from the optimized structures for both states from ab initio calculations (see Section 2.2), the absolute sign of θ can be determined.

2.2. Computational Results

Table 1 collects the structural data, that is, rotational constants (*A*, *B*, and *C*) in the electronic ground (double prime) and excited (single prime) states, their changes upon electronic excitation (ΔA, ΔB, and ΔC), and the respective inertial defects, which are a measure for the nonplanarity of a molecule in a given electronic state and are defined as $\Delta I = I_C - I_A - I_B$. For a planar molecule, the experimentally determined inertial defect is small and negative. The planar equilibrium structures, calculated at the CC2/cc-pVTZ level of theory, both have inertial defects, which are exactly zero, without imposing symmetry constraints in the geometry optimizations. The experimental value contains vibrational corrections from vibrational averaging of the ground- and excited-state structures. The difference in the experimental and calculated ΔI values gives a first-order approximation of the amount of vibrational averaging contained in the experimental rotational constants. We estimate that vibrational contributions to the equilibrium rotational constants are less than 0.1% of the value of the respective rotational constant, that is, a maximum of 3 MHz.

The genuine CC2- and the SCS-CC2-optimized geometries are almost identical for the lowest excited singlet state of 5FI. Herein, CC2 is capable of accurately predicting the geometry parameters of the lowest excited singlet state. In contrast, we found for 5CI[5] that genuine CC2 yielded the reverse adiabatic order of the lowest two $\pi\pi^*$ states compared with SCS-CC2 or SOS-CC2. As a consequence, in this case, only the spin-scaled CC2 variants gave rotational constants and TDM orientations in agreement with our experimental high-resolution spectra.

Table 2 gives the bond lengths of 5FI in the electronic ground state and lowest excited singlet state and their changes obtained from CC2/cc-pVTZ calculations. The bond-lengths changes upon electronic excitation are compared with those of 5CI and indole. The lowest electronically excited singlet state in indole is the L$_b$ state,[23,25–30] whereas recently we

showed that the lowest excited state in 5CI was the L$_a$ state.[5] The bond-length changes in 5FI clearly show that the lowest excited state here is L$_b$, as in indole.

The electronic nature of the excited state can also be deduced from the orientation of the TDM in the molecular frame. For a planar molecule the TDM orientation with respect to the inertial *a*-axis is defined by Equation (1):

$$\mu_a = \mu \cos \theta \tag{1}$$

in which θ is the angle of the transition moment vector with a molecule-fixed *a* axis. The experimentally observed intensities of *a*- and *b*-type transitions in the electronic absorption spectrum are directly proportional to the squares of the projections of the TDM onto the inertial *a* and *b* axes. One cannot, however, distinguish between the two orientations [(I) and (II)] in Figure 2 from the relative intensities of *a* and *b* lines alone, since they have the same projections onto the inertial axes.

Hougen and Watson[32] gave a relationship from which the axis reorientation angle could be computed for any planar molecule by using Cartesian coordinates in the principal axis system of each state [Eq. (2)]:

$$\tan(\theta_T) = \frac{\sum_i m_i \left(a_i' b_i'' - b_i' a_i'' \right)}{\sum_i m_i (a_i' a_i'' - b_i' b_i'')} \tag{2}$$

in which the doubly primed coordinates, a_i'' and b_i'', refer to the coordinates of the *i*th atom in the principal axis system in the electronic ground state; the singly primed coordinates refer to the respective excited-state coordinates; and m_i is the atomic mass of the *i*th atom in the molecule. Using the CC2-optimized structures for the ground and excited states, we obtain an axis reorientation angle of $+0.65°$. We know from the fit of the intensities in the spectrum that if θ_T is positive then θ is necessarily positive and vice versa. Thus, the determination of the sign of θ_T, which can be determined geometrically, provides direct access to the absolute sign of θ, which cannot be determined directly from the experiment, since the observed intensities depend on the squares of the projections along the inertial axes, as described above. The positive direction of angle θ is defined by a counterclockwise rotation of the inertial *a* axis onto the TDM. Therefore, it is orientation (I) in Figure 2 that is observed experimentally. This orientation corresponds to an L$_b$ state in Platt's nomenclature.

Inspection of the leading configurations in the excited-state wave functions shows that the adiabatically lowest state is mainly characterized by HOMO→LUMO excitation (coefficient 0.87), and to a lesser extent by HOMO-1→LUMO+3 (−0.30) and HOMO-1→LUMO (−0.26), see Figure 3. The LUMO+3 is the second unoccupied orbital of π symmetry, while LUMO+1 and LUMO+2 are Rydberg-like orbitals of σ symmetry, located at the NH group and the fluorine atom, respectively. If one compares the frontier orbitals of 5FI with those of 5CI,[5] one sees that the orbital which is HOMO-1 in 5FI changes to HOMO in 5CI and vice versa. The Rydberg orbitals located at the NH group and the fluorine atom in 5FI shift down in energy below the second π^* orbital, whereas in 5CI the Ryd-

Table 2. Bond lengths (in pm) of 5FI in the electronic ground state and lowest excited singlet state at the CC2/cc-pVTZ level of theory and their changes, Δ, in pm upon electronic excitation. For atomic numbering, see Figure 2. The bond-length changes upon excitation to the lowest excited singlet states of 5CI and indole are given for comparison.

	S$_0$	S$_1$	Δ(5CI)	Δ(5CI)[b]	Δ(indole)[a]
N1C2	137.7	142.2	+4.5	±0.0	+4.0
C2C3	137.7	138.1	+0.4	+1.9	+0.6
C3C9	142.8	143.1	+0.3	−2.1	−0.2
C9C4	140.6	140.9	+0.3	+1.6	+0.6
C4C5	138.0	142.4	+4.4	+4.8	+4.6
C5C6	140.2	141.2	+1.0	+3.0	+1.5
C6C7	138.9	142.8	+3.9	+3.4	+3.9
C7C8	139.7	141.0	+1.3	+0.6	+1.2
C8C9	142.3	145.5	+3.2	+4.0	+4.0
C8N1	137.7	135.8	−1.9	+0.6	−1.6
N1H	100.5	100.9	+0.4	±0.0	+0.2
C5F	135.5	134.2	−1.2	–	–

[a] Values obtained at the CC2/cc-pVTZ level of theory.[31] [b] Values obtained at the SCS-CC2/cc-pVTZ level of theory.[5]
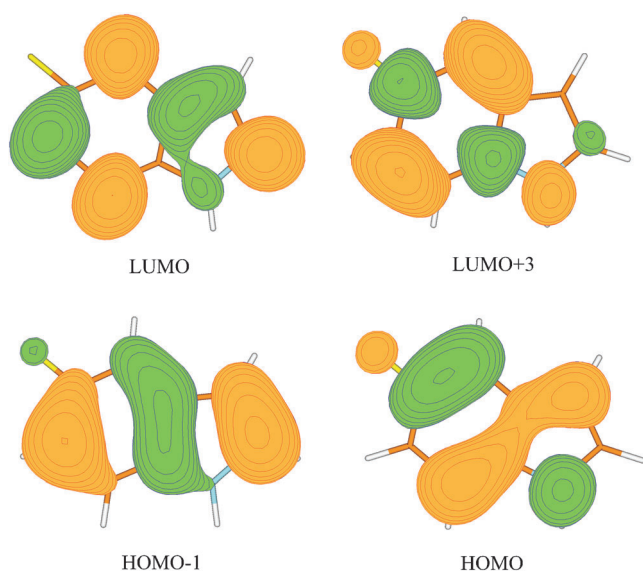
Figure 3. Contour plots of the highest occupied and lowest unoccupied π-type molecular orbitals of 5FI at the optimized S_1 geometry from CC2/cc-pVTZ calculations (isosurface value = 0.03).

berg orbitals are situated above the π^* orbitals. Furthermore, the amplitudes at the fluorine substituent are considerably smaller than those at the cyano substituent.

Recently, we investigated the TDM orientation in 5CI.[5] In this molecule, the TDM is oriented along the *a* axis of the molecule and has to be classified as an L_a-type state. As shown above, the orientation of the TDM in the lowest excited singlet state of 5FI makes an angle of 59° with the *a* axis. This is close to the SCS-CC2-calculated value for the S_2 state of 5CI of 65°. This is further evidence that between 5FI and 5CI the electronic nature of the lowest excited state changes from L_b to L_a. Comparing the structural changes upon excitation, one also finds that the S_1 geometry of 5FI corresponds to the S_2 geometry of 5CI, as calculated at the SCS-CC2 level.

Figure 4 shows a comparison of the density differences between the S_0 and S_1 states of 5FI and between the S_0 and S_2 states of 5CI. According to simple chemical ideas, both substituents would be expected to decrease the electron density of the chromophore, even in the ground state; the cyano group through the $-M$ effect and the fluoro group through the $-I$ effect; however, the density differences for excitation to the respective states are considerably different. In both cases, a net charge flow from the pyrrole to the benzene ring takes place, similar to that in indole itself.[30, 33] However, this charge migration is considerably larger in 5CI than in 5FI, in agreement with the fact that the lowest excitation in 5CI leads to the L_a state.

Averaging the ring charges, obtained from the natural bond orbital (NBO) analysis using the SCS-CC2 wave functions, we find a net charge flow of 0.12 electron charges (e) from the pyrrole ring to the benzene ring upon excitation to the S_1 state of 5FI and of 0.58 e for excitation to the S_2 state of 5CI. The dipole moments of 5CI are 7.1 and 10.1 D in the S_0 and S_2 states, respectively, whereas for 5FI we find much smaller

values of 3.5 and 3.7 D for S_0 and S_1, respectively. Most notably, most of the density differences for the π and σ orbitals at a given center have different signs for 5FI. Also, the importance of electron flow through σ bonds is higher in 5FI than that in 5CI. We attribute this to the fact that the electronic effects of fluorine on the chromophore are purely inductive, whereas the cyano group exerts mesomeric effects.

Furthermore, the zero-point-corrected adiabatic excitation energy (ν_0) of the lowest excited singlet state is given in Table 1. The zero-point-energy-corrected CC2/cc-pVTZ-calculated value of 35 144 cm^{-1} is in fair agreement with the experimental value of 34 336 cm^{-1} (0.1 eV deviation).

3. Conclusions

The rotational constants of the electronic ground state and first excited singlet state of 5FI have been determined for the first time. Very good agreement between the experimental results and results from quantum chemical calculations at the CC2/cc-pVTZ and SCS-CC2/cc-pVTZ levels was obtained. Contrary to the case of 5CI, the CC2 level of theory already yields the correct ordering of the lowest two excited singlet states and the correct TDM orientation for this state. From the orientation of the TDM in the molecular frame, the electronic nature of this excited state was proven to be similar to the L_b state of indole. Density difference plots for the lowest $\pi\pi^*$ excitation in 5FI and the second $\pi\pi^*$ excitation in 5CI showed considerably different charge flows from the pyrrole moiety to the benzene ring upon excitation.
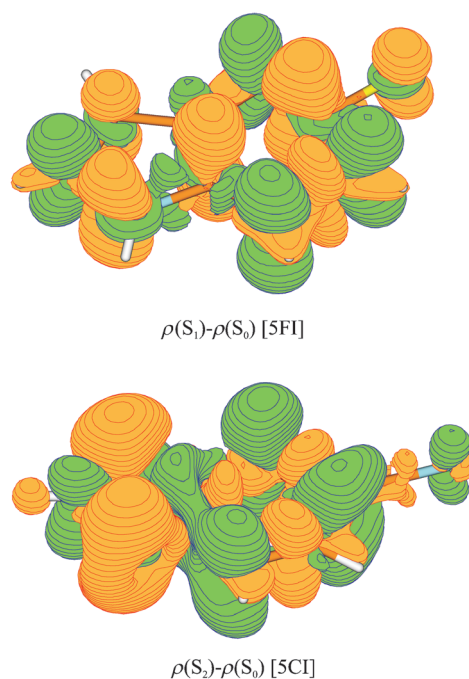

$\rho(S_1)$-$\rho(S_0)$ [5FI]

$\rho(S_2)$-$\rho(S_0)$ [5CI]

Figure 4. Isosurface plots of the density differences, $\Delta\rho$, for 5FI and 5CI from the SCS-CC2/cc-pVTZ calculations (isosurface value = 0.001). Orange and green show regions of decreased and increased electron density, respectively.

[1] J. R. Platt, *J. Chem. Phys.* **1949**, *17*, 484–495.

[2] R. Hoffmann, A. Imamura, W. J. Hehre, *J. Am. Chem. Soc.* **1968**, *90*, 1499–1509.

[3] R. Hoffmann, E. Heilbronner, R. Gleiter, *J. Am. Chem. Soc.* **1970**, *92*, 706–707.

[4] C. Brand, W. L. Meerts, M. Schmitt, *J. Phys. Chem. A* **2011**, *115*, 9612–9619.

[5] O. Oeltermann, C. Brand, B. Engels, J. Tatchen, M. Schmitt, *Phys. Chem. Chem. Phys.* **2012**, DOI: 10.1039/c2cp41094j .

[6] T. L. O. Barstis, L. I. Grace, T. M. Dunn, D. L. Lubman, *J. Phys. Chem.* **1994**, *98*, 4261–4270.

[7] Y. Huang, M. Sulkes, *Chem. Phys. Lett.* **1996**, *254*, 242–248.

[8] M. Schmitt, J. Küpper, D. Spangenberg, A. Westphal, *Chem. Phys.* **2000**, *254*, 349–361.

[9] S. Gerstenkorn, P. Luc, Atlas du spectre d'absorption de La molécule d'iode, CNRS, Paris, **1982**.

[10] R. Ahlrichs, M. Bär, M. Häser, H. Horn, C. Kölmel, *Chem. Phys. Lett.* **1989**, *162*, 165–169.

[11] Turbomole V6.1 2009, a development of University of Karlsruhe and Forschungszentrum Karlsruhe GmbH, **1989–2007**, TURBOMOLE GmbH, since **2007**; available from http://www.turbomole.com.

[12] T. H. Dunning, *J. Chem. Phys.* **1989**, *90*, 1007–1023.

[13] C. Hättig, F. Weigend, *J. Chem. Phys.* **2000**, *113*, 5154–5161.

[14] C. Hättig, A. Köhn, *J. Chem. Phys.* **2002**, *117*, 6939–6951.

[15] C. Hättig, *J. Chem. Phys.* **2003**, *118*, 7751–7761.

[16] A. Hellweg, S. Grün, C. Hättig, *Phys. Chem. Chem. Phys.* **2008**, *10*, 4119–4127.

[17] A. E. Reed, R. B. Weinstock, F. Weinhold, *J. Chem. Phys.* **1985**, *83*, 735–746.

[18] Step-Size Adaptation Based on Non-Local Use of Selection Information, A. Ostermeier, A. Gawelczyk, N. Hansen in Lecture Notes in Computer Science: Parallel Problem Solving from Nature (PPSN III) (Eds.: Y. Davidor, H.-P. Schwefel, R. Männer), Springer, Berlin, **1994**.

[19] N. Hansen, A. Ostermeier, *Evolutionary Computation* **2001**, *9*, 159–195.

[20] C. Brand, O. Oeltermann, D. W. Pratt, R. Weinkauf, W. L. Meerts, W. van der Zande, K. Kleinermanns, M. Schmitt, *J. Chem. Phys.* **2010**, *133*, 024303.

[21] W. L. Meerts, M. Schmitt, *Int. Rev. Phys. Chem.* **2006**, *25*, 353–406.

[22] A. Held, B. B. Champagne, D. W. Pratt, *J. Chem. Phys.* **1991**, *95*, 8732–8743.

[23] G. Berden, W. L. Meerts, E. Jalviste, *J. Chem. Phys.* **1995**, *103*, 9596–9606.

[24] Y. R. Wu, D. H. Levy, *J. Chem. Phys.* **1989**, *91*, 5278–5284.

[25] D. M. Sammeth, S. Yan, L. H. Spangler, P. R. Callis, *J. Phys. Chem.* **1990**, *94*, 7340–7342.

[26] M. R. Eftink, L. A. Selvidge, P. R. Callis, A. A. Rehms, *J. Phys. Chem.* **1990**, *94*, 3469–3479.

[27] B. Albinsson, B. Nordén, *J. Phys. Chem.* **1992**, *96*, 6204–6212.

[28] T. L. O. Barstis, L. I. Grace, T. M. Dunn, D. L. Lubman, *J. Phys. Chem.* **1993**, *97*, 5820–5825.

[29] B. J. Fender, D. M. Sammeth, P. R. Callis, *Chem. Phys. Lett.* **1995**, *239*, 31–37.

[30] C. Kang, T. M. Korter, D. W. Pratt, *J. Chem. Phys.* **2005**, *122*, 174301.

[31] C. Brand, J. Küpper, D. W. Pratt, W. L. Meerts, D. Krügler, J. Tatchen, M. Schmitt, *Phys. Chem. Chem. Phys.* **2010**, *12*, 4968–4997.

[32] J. T. Hougen, J. K. G. Watson, *Can. J. Phys.* **1965**, *43*, 298.

[33] P. R. Callis, *J. Chem. Phys.* **1991**, *95*, 4230.